Twenty-Seventh Symposium (International) on Combustion/The Combustion Institute, 1998/pp. 2249–2257

SIMULATION OF THE TRANSIENT, COMPRESSIBLE, GAS-DYNAMIC BEHAVIOR OF CATALYTIC-COMBUSTION IGNITION IN STAGNATION FLOWS

LAXMINARAYAN L. RAJA,[1] ROBERT J. KEE[1] and LINDA R. PETZOLD[2]

[1]*Engineering Division*
Colorado School of Mines
Golden, CO 80401, USA
[2]*Computational Science & Engineering Program*
Department of Mechanical & Environmental Engineering
University of California, Santa Barbara
Santa Barbara, CA 93106, USA

This paper develops and uses a computation model to explore the transient ignition dynamics of catalytic combustion in a stagnation-flow configuration. The analysis considers the elementary heterogeneous chemistry associated with catalytic behavior at the surface. It also considers gas-dynamic effects in the boundary layer, including temporal and spatial pressure variations. The gas-dynamic effects are included through the axial momentum equation, which has been neglected in previous analyses of unsteady stagnation flows. In addition to the physical interpretation of ignition transients, the paper presents a mathematical and computational analysis and comparison of the constant-pressure and compressible stagnation-flow equations. The constant-pressure equations, as commonly formulated and used, are a system of differential-algebraic equations (DAE) that have an index greater than two. This high-index behavior is responsible for severe numerical difficulties in regions of fast transients or stringent numerical error control. This paper relaxes the constant-pressure assumption using a compressible-flow formulation, which extends the range of physical validity and reduces the index of the transient stagnation-flow problem while preserving stagnation-flow "similarity."

Introduction

Catalytic combustion is emerging as a practical technology [1–4], increasing the need for fundamental understanding of the heterogeneous chemistry at the catalyst surface and the fluid-mechanical interactions in the adjacent boundary layers. The stagnation flow of a combustible gas over a flat catalytic surface serves as an ideal research platform on which to develop new understanding. The configuration is accessible to a variety of diagnostics and can be simulated using a one-dimensional similarity formulation. This situation is analogous to the burner-stabilized flames and opposed-flow flames that have been used successfully to study gas-phase combustion chemistry.

With the exception of Deutschmann [5,6], previous studies of catalytic combustion in the stagnation-flow configuration have considered the steady-state behavior. Vlachos and colleagues [7,8] have developed models that use continuation methods to describe the bifurcations associated with ignition and extinction behavior. All previous investigations have relied on a constant-pressure formulation.

This paper focuses on the transient behavior of stagnation flows, especially the very fast transients driven by the heterogeneous ignition. Fast transients, which have heretofore been neglected in models of combustion stagnation flows, are seen to trigger compressible gas-dynamic behavior. The constant-pressure equations are systems of differential-algebraic equations (DAE) that are characterized as high-index systems. As such, numerical solution can be unstable during periods of rapid transient behavior. We introduce a compressible-flow formulation that improves the physical representation and reduces the DAE index, which facilitates numerical solution.

There is a growing interest in the transient behavior of unsteady laminar flames [9–14]. The objective is to understand flame structure in time-varying strain fields, thus extending laminar-flamelet concepts in turbulent combustion. In the usual constant-pressure formulation, numerical difficulties associated with high-index DAEs are easily triggered. The approach developed herein applies directly to this larger class of problems.

Compressible Stagnation-Flow Equations

Derivation of the compressible stagnation-flow equations follows a procedure that is analogous to

deriving the constant-pressure equations [15,16]. Beginning with the full axisymmetric fluid-mechanical conservation equation, we first conjecture that the solutions are functions of time t and the axial coordinate x in the following form: axial velocity $u = u(t, x)$, scaled radial velocity $v/r = V(t, x)$, temperature $T = T(t, x)$, and mass fractions $Y_k = Y_k(t, x)$. Boundary conditions are applied at two values of x and have no radial dependence. After some manipulation of the momentum equations, it can be shown that $1/r\ \partial p/\partial r = \Lambda(t)$ is a function of t alone. The system of compressible equations is stated as:

Mass continuity:

$$\frac{\partial \rho}{\partial t} + \frac{\partial}{\partial x}(\rho u) + 2\rho V = \frac{\rho}{p_{\text{tot}}}\frac{\partial p}{\partial t} - \frac{\rho}{T}\frac{\partial T}{\partial t} - \rho\bar{W}\sum \frac{1}{W_k}\frac{\partial Y_k}{\partial t} + \frac{\partial}{\partial x}(\rho u) + 2\rho V = 0 \quad (1)$$

Axial momentum:

$$\rho\frac{\partial u}{\partial t} + \rho u\frac{\partial u}{\partial x} + \frac{\partial p}{\partial x} - 2\mu\frac{\partial V}{\partial x} - \frac{4}{3}\frac{\partial}{\partial x}\left(\mu\frac{\partial u}{\partial x}\right) + \frac{4}{3}\frac{\partial}{\partial x}(\mu V) = 0 \quad (2)$$

Scaled radial momentum:

$$\rho\frac{\partial V}{\partial t} + \rho u\frac{\partial V}{\partial x} - \frac{\partial}{\partial x}\left(\mu\frac{\partial V}{\partial x}\right) + \rho V^2 + \Lambda = 0 \qquad V \equiv \frac{v}{r}, \quad \Lambda \equiv \frac{1}{r}\frac{\partial p}{\partial r} = \Lambda(t) \quad (3)$$

Thermal energy:

$$\rho c_p\frac{\partial T}{\partial t} + \rho c_p u\frac{\partial T}{\partial x} - \frac{\partial p}{\partial t} - u\frac{\partial p}{\partial x} - \frac{\partial}{\partial x}\left(\lambda\frac{\partial T}{\partial x}\right) + \rho\sum c_{pk}Y_k V_k\frac{\partial T}{\partial x} + \sum \dot{\omega}_k h_k = 0 \quad (4)$$

Gas-phase species conservation:

$$\rho\frac{\partial Y_k}{\partial t} + \rho u\frac{\partial Y_k}{\partial x} + \frac{\partial}{\partial x}(\rho Y_k V_k) - \dot{\omega}_k W_k = 0 \quad (k = 1, \ldots K_g) \quad (5)$$

Equation of state:

$$\rho = \frac{p_{\text{tot}}\bar{W}}{RT}, \qquad p_{\text{tot}} = p_{\text{ref}} + p \quad (6)$$

Variables include: $\dot{\omega}_k$, molar production rate by gas-phase chemical reaction; ρ, the mass density; W_k, molecular mass of species; c_p specific heat; μ, dynamic viscosity; and λ, thermal conductivity. The total thermodynamic pressure p_{tot} is the sum of a reference pressure p_{ref} and a varying pressure p, which is the dependent variable. The diffusion velocity is

$$V_k = \frac{1}{X_k\bar{W}}\sum W_j D_{kj}\frac{\partial X_j}{\partial x} - \frac{D_k^T}{\rho Y_k}\frac{1}{T}\frac{\partial T}{\partial x} \quad (7)$$

where X_k are the mole fractions, D_{kj} are the ordinary multicomponent diffusion coefficients, and D_k^T are the thermal diffusion coefficients. In the mass-continuity equation, $\partial\rho/\partial t$ is expanded through the equation of state in terms of the dependent variables, which facilitates the coupling of pressure as a dependent variable.

Constant-Pressure Equations

The constant-pressure equations are a subset of the compressible equations (equations 1,3–6). The pressure is not a dependent variable, but rather a parameter used in the equation of state. Hence, the pressure derivatives are not retained in the continuity or thermal-energy equations. The axial-momentum equation is decoupled from the system, and most investigators neglect it. The nomenclature "constant-pressure" is a slight misnomer, since an axial pressure distribution can be determined and the radial pressure gradient is retained through Λ.

Boundary Conditions

The boundary conditions describe the flow between an inlet plane ($x = L$) and a solid surface ($x = 0$), which is chemically reactive. However, the essential features of the compressible-flow formulation and the numerical methods do not depend on the particular boundary conditions. At the inlet plane ($x = L$), $u = u_{\text{in}}(t)$, $v/r = V_{\text{in}} = 0$, $T = T_{\text{in}}(t)$, and $Y_k = Y_{k,\text{in}}(t)$. The pressure is fixed at the inlet plane to be the reference pressure, thus $p = 0$.

At the stagnation surface ($x = 0$), $v/r = V = 0$, and $T = T_s(t)$. If the surface is nonreactive, then the surface-normal velocity vanishes $u_s = 0$ and $\rho Y_k V_k = 0$, that is, there is no net mass flux through the boundary. When the boundary is reactive, the boundary conditions are more complex. The chemical state of the surface must be included as dependent variables and a heterogeneous chemical reaction mechanism is needed [17–19,25]. The surface state, in terms of the site fractions Z_k, is described by

$$\frac{\partial Z_k}{\partial t} - \frac{\dot{s}_k}{\Gamma} = 0 \quad (k = 1, \ldots K_s) \quad (8)$$

where $\dot{s}_k$ is the molar production rate of surface species by heterogeneous reaction and Γ is the molar density of potentially available surface sites ($\Gamma = 2.71(10^{-9})$ mol/cm^2 for platinum). The coupling between the gas phase and the surface is established through a mass-flux matching condition for each of the gas-phase species as $\rho Y_k(u_{\text{st}} + V_k) = \dot{s}_k W_k$. The Stefan velocity is nonzero when there is net mass exchange between the gas and the surface;

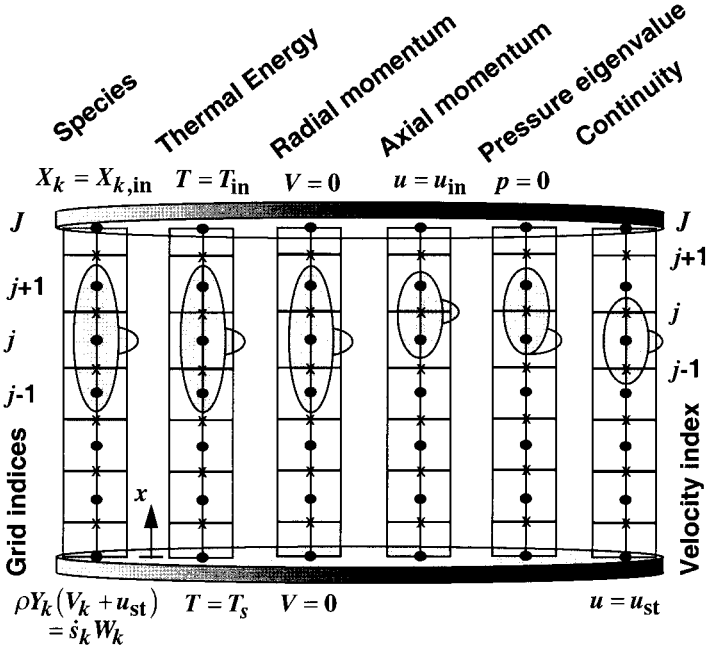

FIG. 1. Finite-volume, staggered-grid, spatial-difference stencil for the compressible stagnation-flow equations. Grid points, which are at control-volume centers, are used to represent all dependent variables except axial velocity, which is represented at the control-volume faces. The grid indices are shown on the left and the face indices on the right. The right-facing protuberance on the stencils indicates where the time derivative is evaluated. For the pressure-eigenvalue equation there is no time derivative, indicated by an unfilled protuberance.

$u_{\text{st}} = (1/\rho) \Sigma \dot{s}_k W_k$, where the summation includes the gas-phase species that participate in the surface reactions. The transient surface temperature is determined from an energy balance as

$$\rho_s c_p V \frac{dT_s}{dt} = \sum \rho h_k (Y_k V_k + Y_k u)_s - \lambda \left(\frac{dT}{dx}\right)_s + 2\sigma\varepsilon(T_s^4 - T_\infty^4) + \dot{P} \qquad (9)$$

where $\rho_s c_p V$ is the thermal capacity of the surface, h_k is the enthalpy of the gas-phase species, ε is the surface emissivity, and $\dot{P}$ is (electrical) power supplied to the surface.

Numerical Method

The numerical method is a method-of-lines approach using control-volume spatial differencing. The time integration is done using DASSL, which implements an implicit, variable-order, variable-step method based on the BDF method [20].

The spatial-difference stencil (Fig. 1) uses a staggered grid in which the axial velocities are represented on the control-volume faces, and all other variables are represented at the control-volume centers (nodes) [21]. The nodes are separated by Δx, which is variable. The inlet at the top and the solid surface at the bottom correspond to nodes and the faces are halfway between nodes. The first axial velocity (face 1) is evaluated just above the surface at $x = \Delta x/2$. The inlet velocity, however, is taken at the top node ($j = J$).

The species-conservation, thermal-energy, and radial-momentum equations are spatially second order and use a conservative central-difference method for the diffusion terms and smooth upwinding for the convective terms. The continuity equation is spatially first order and uses a central-difference formulation for $\partial(\rho u)/\partial x$, with u at the control-volume faces. The axial-momentum equation is second order in velocity and first order in the pressure. The second order comes from the normal-stress term, which is negligible except perhaps very close to the surface or during very rapid transients. Consequently, the spatial differencing uses a first-order one-sided stencil, with the convective term upwinded while the pressure gradient is central differenced using the two nodes that span the face where $\partial u/\partial t$ is evaluated. The normal-stress term is central differenced but can be thought of as a source or sink term. A trivial differential equation $\partial \Lambda/\partial x = 0$ keeps the iteration matrix banded.

The boundary conditions for T and V require specified values at both boundaries. At the inlet boundary, the axial velocity is specified as $u = u_{\text{in}}$, which serves as the boundary condition for the axial-momentum equation. Also, at the inlet boundary, the pressure is taken to be the constant reference pressure, $p_{\text{tot}} = p_{\text{ref}}$, or $p = 0$. This serves as the boundary condition associated with the pressure-curvature equation Λ, which is an implicit boundary condition; that is, there is no explicit boundary condition for Λ itself. At the inlet plane, the continuity equation is

itself solved and does not require a boundary condition.

At the stagnation surface, the axial velocity serves as the boundary condition for the continuity equation. For a nonreactive surface, $u = 0$; for a reactive surface, $u = u_{st}$. At the stagnation surface, the pressure-curvature equation itself is solved, as is the axial-momentum equation at the face just above the surface. Therefore, neither require a boundary condition at the surface.

When the surface is reactive, the flux of gas-phase species to and from the surface is determined from the heterogeneous surface chemistry. The boundary condition is implemented as mass fluxes into (or out of) the half control volume that spans from the stagnation surface to half the distance to the first interior grid point (Fig. 1). A species mass balance leads to a differential equation for the gas-phase species at the surface rather than at the algebraic flux-matching condition $\rho Y_k(u_{st} + V_k) = \dot{s}_k W_k$. There are significant numerical benefits of differential equations for boundary values that can experience rapid variations. The energy balance (equation 9) serves as the boundary condition for the surface temperature.

Because the central differencing on the continuity equation is only neutrally stable, we introduce an artificial damping term to assist numerical stability [22]. Following common practice in solving Euler equations, we add a first-order damping term to the continuity equation

$$\sigma(\Delta x)\,\frac{\partial^2 p}{\partial x^2}$$

using $\sigma = 0.1$.

Differential-Algebraic Equations

A brief explanation of DAEs will facilitate a further mathematical discussion of the stagnation-flow equations. In general, DAEs are stated as a vector residual equation $F(t, w, w') = 0$, where w is the dependent-variable vector and the prime denotes a time derivative. For our purposes, it will be convenient to consider a restricted class of DAEs called semiexplicit nonlinear DAEs, which are represented as

$$\begin{aligned} y' &= f(t, y, z) \\ 0 &= g(t, y, z) \end{aligned} \qquad (10)$$

where the dependent-variable vector is now $w = (y, z)^T$, indicating that some of the dependent variables (y) have time derivatives that can be isolated, whereas others (z) do not. The second equation can be thought of as an algebraic constraint on the differential equations represented by the first equation. The index of the DAE system depends on the derivatives of the constraint equation. If the matrix $\partial g/\partial z$ is nonsingular, then the constraints can in principle be solved for z in terms of y and t. The resulting expression could be substituted into the differential equation 10, yielding a system of ordinary differential equations. Such a system is index one. If, however, $\partial g/\partial z$ is singular then the index is two or higher. By definition, the index of a DAE system $F(t, w, w') = 0$ is equal to the number of times that all or part of the system must be differentiated with respect to t to determine w' as a continuous function of t and w [20]. There are a number of practical problems in the numerical solution of high-index DAEs. The error control in automatic codes like DASSL [20] is designed only for index-one systems and must be modified to handle the index-two case. Furthermore, the condition number of the iteration matrix in implicit numerical methods is $O(h^{-v})$, where h is the timestep and v is the index. Therefore, the numerical methods can fail to converge when they choose the small timesteps required to resolve fast transients accurately [20].

With the brief discussion of index, it is now possible to identify and compare some aspects of the high-index behavior of the constant-pressure and the compressible stagnation-flow equations. To understand the structure of the DAE system, we first identify all variables that are not time differentiated, that is, the z vector. In the constant-pressure formulation, neither the axial velocity u nor the pressure curvature Λ have time derivatives. By introducing the axial momentum equation, the compressible formulation introduces $\partial u/\partial t$. To be of value in reducing the index, however, the momentum equation must be coupled to the other equations. The coupling is accomplished through pressure, which is included as a dependent variable. The variable Λ is not time differentiated in either formulation.

The boundary conditions that simply specify a value, for example, $T = T_{in}$, are seen as simple constraints that raise the index to one, and simple constraints usually cause no trouble. On the other hand, time-varying boundary conditions, for example, $T = T_{in}(t)$, can be more troublesome, especially if they are principally responsible for transient behavior in the solution. In these cases, it is advisable to solve a differential equation for the boundary value (like equation 9), rather than specify a time-varying constraint.

The continuity equation *at the inlet boundary* can be viewed as a constraint equation. Referring to the difference stencil (Fig. 1), it is seen that this first-order equation itself is evaluated at the boundary, and no explicit boundary condition is needed. Moreover, since the inlet temperature, pressure, and composition are specified, the density is fixed and thus $\partial\rho/\partial t = 0$. Therefore, at the boundary, the continuity equation (equation 1) has no time derivative; that is, it is an algebraic constraint. There is no explicit boundary condition for Λ. At the inlet boundary, the

TABLE I
Surface chemistry reaction mechanism for the catalytic reaction of methane–oxygen on platinum

	Reaction	A* (cm, mol, s)	β	E (kJ/mol)
1.	$H_2 + 2Pt(s) \Rightarrow 2H(s)$ FORD/Pt(s) 1/¥	4.46E10	0.5	0
2.	$2H(s) \Rightarrow H_2 + 2Pt(s)$ COV/H(s) 0 0 −6000/†	3.70E21	0.0	67.4
3.	$H + Pt(s) \Rightarrow H(s)$	1.00‡	0.0	0
4.	$O_2 + 2Pt(s) \Rightarrow 2O(s)$	21.0‡	−1.0	0
5.	$2O(s) \Rightarrow O_2 + 2Pt(s)$ COV/O(s) 0 0 −60000/	3.70E21	0.0	213.2
6.	$O + Pt(s) \Rightarrow O(s)$	1.00‡	0.0	0
7.	$H_2O + Pt(s) \Rightarrow H_2O(s)$	0.75‡	0.0	0
8.	$H_2O(s) \Rightarrow H_2O + Pt(s)$	1.00E13	0.0	40.3
9.	$OH + Pt(s) \Rightarrow OH(s)$	1.00‡	0.0	0.0
10.	$OH(s) \Rightarrow OH + Pt(s)$	1.00E13	0.0	192.8
11.	$H(s) + O(s) = OH(s) + Pt(s)$	3.70E21	0.0	11.5
12.	$H(s) + OH(s) = H_2O(s) + Pt(s)$	3.70E21	0.0	17.4
13.	$OH(s) + OH(s) = H_2O(s) + O(s)$	3.70E21	0.0	48.2
14.	$CO + Pt(s) \Rightarrow CO(s)$ FORD/Pt(s) 2/	1.62E20	0.5	0
15.	$CO(s) \Rightarrow CO + Pt(s)$	1.00E13	0.0	125.5
16.	$CO_2(s) \Rightarrow CO_2 + Pt(s)$	1.00E13	0.0	20.5
17.	$CO(s) + O(s) \Rightarrow CO_2(s) + Pt(s)$	3.70E21	0.0	105.0
18.	$CH_4 + 2Pt(s) \Rightarrow CH_3(s) + H(s)$ FORD/Pt(s) 2.3/	4.63E20	0.5	0.0
19.	$CH_3(s) + Pt(s) \Rightarrow CH_2(s) + H(s)$	3.70E21	0.0	20.0
20.	$CH_2(s) + Pt(s) \Rightarrow CH(s) + H(s)$	3.70E21	0.0	20.0
21.	$CH(s) + Pt(s) \Rightarrow C(s) + H(s)$	3.70E21	0.0	20.0
22.	$C(s) + O(s) \Rightarrow CO(s) + Pt(s)$	3.70E21	0.0	628.0
23.	$CO(s) + Pt(s) \Rightarrow C(s) + O(s)$	1.00E18	0.0	184.0

*Rate expressions in the form $k = AT^{\beta} \exp(-E/RT)$.

‡Sticking coefficient: $\gamma = AT^{\beta} \exp(-E/RT)$, $k = \gamma/\Gamma^{m} \sqrt{RT/2\pi W}$.

¥The order for forward rate of progress is modified as indicated.

†Rate expression modified by an activated coverage dependence as $k = AT^{\beta} \exp(-E/RT) \times \{10^{\eta[Z]}[Z]^{\mu} \exp(\varepsilon[Z]/RT)\}$, where Z is the site fraction of the named species and η, μ, and ε are the three coverage parameters. Here $\varepsilon = -6000$.

value of Λ must be determined in such a way that all the other boundary conditions are satisfied. Being an eigenvalue, Λ's effect is felt through its influence on the V velocity in the radial momentum equation, and subsequently by V's influence on u through the continuity equation.

We have shown that the DAE system corresponding to the discrete form of the compressible-stagnation-flow equations is of Hessenberg-index-two structure [20], which is represented by equation 10. The constraint g does not depend on z, and the matrix $\partial g/\partial y \ \partial f/\partial z$ is nonsingular. Here, Λ is the only index-two variable (i.e., it plays the role of z).

It is possible and beneficial to reduce the system to index one by replacing Λ with a new dependent variable ϕ, where $\Lambda \equiv \partial\phi/\partial t$ [23]. The initial condition for ϕ is arbitrary because ϕ itself never appears in the equations—a suitable choice is $\phi = 0$. Anywhere Λ appears, we simply replace it with $\partial\phi/\partial t$, which is conveniently done in DAE software. The index reduction can be seen from the following procedure. The continuity at the inlet boundary (an algebraic constraint) can be differentiated once with respect to t to yield an equation for $\partial V/\partial t$. Then, $\partial V/\partial t$ is replaced by substitution of the radial-momentum equation. This substitution introduces $\Lambda \equiv \partial\phi/\partial t$, which makes the continuity equation (at the inlet boundary) an independent differential equation for ϕ. Thus, the modified system is index one. This set of substitutions is not actually done in practice—it simply must be possible to do them to achieve the index reduction.

Catalytic Ignition

We have chosen to simulate atmospheric-pressure catalytic ignition on a platinum foil using conditions investigated by Deutschmann [5]. The surface-reaction mechanism (Table 1) is taken directly from Deutschmann [5,24], who validated it experimentally using ignition-temperature data. The inlet flow conditions used here are $u_{in} = 8$ cm/s, $T_{in} = 300$ K, an inlet mixture of 3% CH_4, 3% O_2, and 94% N_2. The inlet-to-catalyst separation is 5 cm. The catalyst surface is initially covered by oxygen.

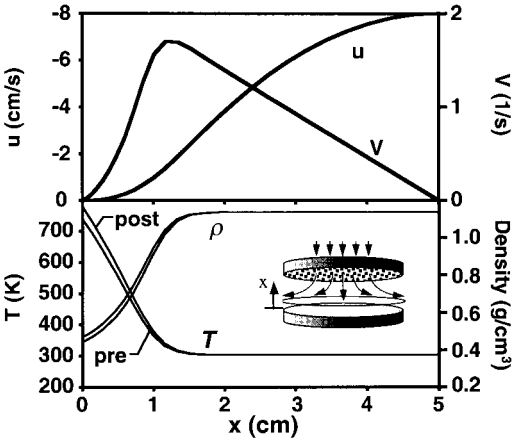

FIG. 2. Velocity, temperature, and density profiles before and after catalytic ignition on a platinum foil. Conditions are 5-cm separation between inlet and surface, atmospheric pressure, 8 cm/s inlet velocity, 300 K inlet temperature, inlet mixture composition 3% CH_4, 3% O_2, and 94% N_2.

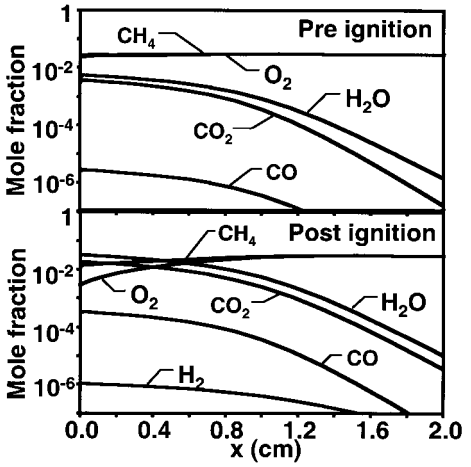

FIG. 3. Gas-phase species profiles before and after catalytic ignition on a platinum foil. Conditions are the same as Fig. 2.

The simulations follow Deutschmann's experimental procedure, which is as follows. The inlet flow is held steady while the foil is heated electrically, raising its temperature in small steps. The foil temperature is permitted to stabilize before it is again raised. When ignition conditions are reached, the surface temperature increases rapidly by combustion heating. The system then approaches a steady catalytic-burning condition.

The simulations presented here use a mesh of 60 points that are nonuniformly placed by a power-law

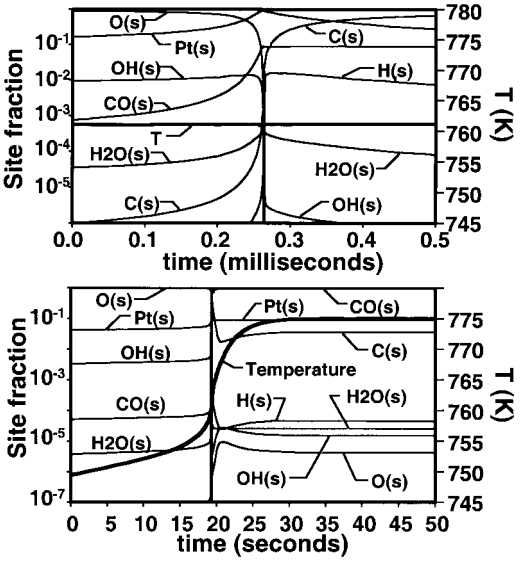

FIG. 4. Transient surface-state composition during catalytic ignition, shown on two timescales. Conditions are the same as for Fig. 2. The zero point for the abscissa scale is arbitrary.

stretching from the surface. The first grid point is $1.44(10^{-3})$ cm from the stagnation surface and the last grid interval at the top inlet boundary is 0.12 cm. In these simulations the gas-phase chemistry has been entirely suppressed, which is appropriate for very lean mixtures and low temperatures.

Figure 2 shows the steady gas-phase velocity and temperature profiles before and after ignition, and Fig. 3 shows the corresponding species profiles. Because of the experimental procedure that slowly raises the surface temperature, a thermal boundary layer has been established prior to ignition. Due to the elevated surface temperature, there is some preignition chemistry that affects the species profiles. Because the mixture is so dilute, the temperature rise associated with the ignition is only around 50 °C. Nevertheless, as shown later, there are still considerable gas-dynamic effects associated with this relatively weak ignition.

Figure 4 shows the transient response of the surface state throughout the ignition event. Clearly, there are two important timescales. The longer timescale (seconds) is illustrated by the temperature response, which is governed principally by the thermal inertia of the foil itself (equation 9). The shorter timescale (microseconds) is characterized by the heterogeneous chemical behavior.

The ignition is triggered by the net desorption of oxygen from the surface at the ignition temperature (reactions 4 and 5). Once there are open platinum sites available, CH_4 is adsorbed rapidly, followed by a sequence of reactions that produce CO, CO_2, and

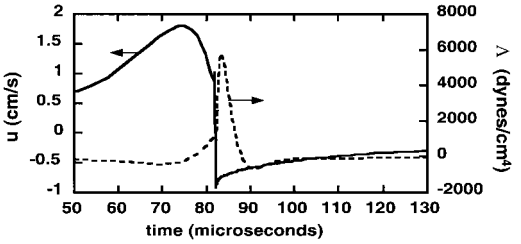

FIG. 5. Transient response of the Stefan velocity and the pressure-curvature eigenvalue during the ignition transient for the conditions of Fig. 2. The zero point for the abscissa scale is arbitrary.

H_2O, which subsequently desorb into the boundary layer.

Consider now the gas-dynamic effects that are driven by the rapid chemistry on the surface. Fig. 5 shows the transient response of the Stefan velocity at the surface, which initially rises "slowly" to a value of nearly 2 cm/s as the oxygen desorbed. The extremely sharp decrease to a negative velocity of around 1 cm/s is caused by the rapid CH_4 adsorption. Finally, the Stefan velocity returns to zero as the new burning steady state is established and there is no net mass exchange at the boundary. The ignition behavior, which occurs on a timescale of a few hundred microseconds excites an acoustic response in the gas. The Stefan velocities, first positive, then negative, then returning to zero, act as a "piston" that drives a pressure response in the flow as seen in the Λ behavior.

The fastest transient is caused by the rapid adsorption of CH_4 as the surface sites open (reaction 18). Reaction 18 is equivalent to a CH_4 sticking coefficient of 0.01, but with a reaction order of 2.3 for the open platinum sites. Deutschmann determined that the 2.3 reaction order was necessary to predict his ignition-temperature data [6]. The relatively high reaction order causes the CH_4 adsorption to proceed on a timescale of around 0.1 μs, once there are sufficient open sites available. This in turn drives the very fast negative transient in the Stefan velocity.

It is unlikely that an actual surface could be maintained so perfectly uniform that all points on the surface would ignite at exactly the same time as implied by the one-dimensional similarity behavior. Instead, because of heterogeneities on the surface, the apparent adsorption rate would be reduced. Consequently, the strength of the gas-dynamic response would be reduced. Indeed, the simulations show that when the CH_4 adsorption rate is reduced, the gas-dynamic response is moderated. Even though the ignition events simulated here may be stronger than actual events, the numerical method performed very well in representing extremely rapid transients. Furthermore, even with reduced ignition times, there remain significant gas-dynamic responses that should be represented in models.

Behavior of the Numerical Method

Introduction of the compressible-flow formulation, together with numerical implementation, leads to robust simulations for extremely fast transients. The timesteps reduce appropriately to capture high-frequency details of the solution. Moreover, there are essentially no convergence failures, indicating that the numerical method remains well conditioned even for extremely small timesteps. This behavior demonstrates in practical terms that the system has been successfully reduced to index one, confirming the analytical result.

The constant-pressure formulation is high index even with implementation of ϕ instead of Λ as the dependent variable. This results from the absence of any time derivatives for u. Attempts to solve the methane-ignition problem with the constant-pressure formulation were generally unsuccessful, except by significantly relaxing the error control on Λ and u. Even then, although the solutions appear generally correct, they exhibit unstable behavior near fast transients, particularly on Λ.

In addition to the catalytic-ignition problem, we developed several model problems that helped identify and ameliorate the high-index problems. One of these oscillated the inlet flow, and another forced a sharp rise in the surface temperature. Although the constant-pressure approach was successful for low-frequency and low-amplitude oscillations and relatively shallow temperature ramps, it was easy to cause numerical failures for fast transients.

In the method described here, we do not seek to capture details of the acoustic-wave behavior accurately. Instead, our intent is to obtain stable solutions during the fast ignition transients. By applying upwind differencing for the advection terms and including first-order artificial damping, we use spatial differencing that is relatively diffusive. Any method that seeks to simulate the pressure response accurately must be nondissipative and nondispersive, which usually requires high-order differencing and high mesh resolution.

Limitation of the Stagnation-Flow Formulation

By assumption, the stagnation-flow similarity formulation presumes infinite radial extent. In reality, the stagnation-flow similarity breaks down at some finite radius beyond which the flow merges smoothly with an ambient flowfield. Although the stagnation-flow equations accommodate the axial pressure variations, the radial pressure field Λ is presumed to always have a parabolic distribution. In reality, the

radial pressures must adjust to transient conditions, which requires acoustic communication with the ambient flow. Thus, there is only a finite radius over which the similarity is valid, and that radius decreases as transients become faster.

Summary and Conclusions

A compressible-flow formulation of the stagnation-flow problem is shown to improve physical models of the fast transient response associated with events like catalytic ignition. This formulation, together with improved numerical algorithms, reduce the DAE index of the transient stagnation-flow problem, which significantly improves computational accuracy and stability.

Acknowledgments

We are grateful to Dr. Olaf Deutschmann, who generously shared with us considerable insight and experience from his earlier research. This work was supported by NASA, through the CCACS program at the Colorado School of Mines.

REFERENCES

1. Pfefferle, L. D. and Pfefferle, W. C., *Catal. Rev.—Sci. Eng.* 29:219–267 (1987).
2. Farrauto, R. J., Larkin, M., Fu, J., and Feeley, J., *Mater. Res. Soc. Symp. Proc.* 344:101–120 (1994).
3. Dalla Betta, R. A., Schlatter, J. C., Nikolas, S. G., Razdan, M. K., and Smith, D. A., *International Gas Turbine and Aeroengine Congress and Exposition,* ASME 95-GT-65, Houston, TX, 1995.
4. Beebe, K. W., Cutrone, M. B., Matthews, R. N., Betta, R. A. D., Schlatter, J. C., Furuse, Y., and Tsuchiya, T., *International Gas Turbine and Aeroengine Congress and Exposition,* ASME 95-GT-137, Houston, TX, June 5–8, 1995.
5. Deutschmann, O., Schmidt, R., Behrendt, F., and Warnatz, J., in *Twenty-Sixth Symposium (International) on Combustion,* The Combustion Institute, Pittsburgh, 1996, pp. 1747–1754.
6. Deutschmann, O., "Modellierung von Reaktionen an Oberflaechen und Deren Kopplung mit Chemisch Reagierenden Stroemungen," Ph.D. thesis, University of Heidelberg, 1996.
7. Bui, P.-A., Vlachos, D. G., and Westmoreland, P. R., *Surf. Sci.* 385:L1029–L1034 (1997).
8. Bui, P.-A., Vlachos, D. G., and Westmoreland, P. R., *Ind. Eng. Chem. Res.* 36:2558–2567 (1997).
9. Egolfopoulos, F. N. and Campbell, C. S., *J. Fluid Mech.* 318:1–29 (1996).
10. Stahl, G. and Warnatz, J., *Combust. Flame* 85:285–299 (1991).
11. Sung, C. J. and Law, C. K., *37th Aerospace Sciences Meeting,* AIAA Paper 98-0555, Reno, NV, January 12–15, 1998.
12. Im, H. G., Law, C. K., Kim, J. S., and Williams, F. A., *Combust. Flame* 100:21–30 (1995).
13. Im, H. G., Chen, J. H., and Chen, J.-Y., *Western States Section/The Combustion Institute,* WSS/CI 97F-111, Diamond Bar, CA, October 23–24, 1997.
14. Kistler, J. S., Sung, C. J., Kreutz, T. G., Law, C. K., and Nishioka, M., in *Twenty-Sixth Symposium (International) on Combustion,* The Combustion Institute, Pittsburgh, 1996, pp. 113–120.
15. Dixon-Lewis, G., in *Twenty-Third Symposium (International) on Combustion,* The Combustion Institute, Pittsburgh, 1990, pp. 305–324.
16. Kee, R. J., Miller, J. A., Evans, G. H., and Dixon-Lewis, G., in *Twenty-Second Symposium (International) on Combustion,* The Combustion Institute, Pittsburgh, 1988, pp. 1479–1494.
17. Coltrin, M. E., Kee, R. J., and Rupley, F. M., *Int. J. Chem. Kinet.* 23:1111–1128 (1991).
18. Meeks, E., Kee, R. J., Dandy, D. S., and Coltrin, M. E., *Combust. Flame* 92:144–160 (1993).
19. Warnatz, J., Allendorf, M. D., Kee, R. J., and Coltrin, M. E., *Combust. Flame* 96:393–406 (1994).
20. Brenan, K. E., Campbell, S. L., and Petzold, L. R., *Numerical Solution of Initial-Value Problems in Differential Algebraic Equations,* 2nd ed. SIAM, Philadelphia, PA, 1996.
21. Patankar, S. V., *Numerical Heat Transfer and Fluid Flow,* Hemisphere, New York, 1980.
22. Jameson, A. and Yoon, S., *AIAA J.* 24:1737–1743 (1986).
23. Ascher, U. M. and Petzold, L. R., *Computer Methods for Ordinary Differential Equations and Differential-Algebraic Equations,* SIAM, Philadelphia, 1998.
24. Hickman, D. A. and Schmidt, L. D., *AIChE J.* 39:1164–1177 (1993).
25. Coltrin, M. E., Kee, R. J., Rupley, F. M., and Meeks, E., *Surface CHEMKIN-III: A Fortran Package for Analyzing Heterogeneous Chemical Kinetics at a Solid-Surface—Gas-Phase Interface,* Sandia report SAND96-8217.

COMMENTS

Olaf Deutschmann, University of Minnesota, USA. For a sufficiently slow transient, are there differences between solutions using the incompressible and compressible formulation?

Author's Reply. The original incompressible formulation is physically valid only in the low Mach number limit. The implementation of this limit in the flow model is by filtering out the pressure as a dependent variable from the flowfield representation. Hence, the thermodynamic pressure that enters the equation of state is a constant. As explained in the paper, this leads to a high-index behavior of the resulting differential-algebraic equations (DAE), particularly for fast transients. The compressible formulation simply reintroduces the pressure as a dependent variable and retains the axial momentum equation as a governing equation. Mathematically, this lowers the DAE index. For low Mach number flows, axial pressure variations determined by the axial momentum equation is negligible compared to the absolute value of the pressure that enters the equation of state. Also, for slow enough transients, the time derivative terms in the continuity equation are negligible compared to the remaining terms. Hence, the compressible formulation gives the same solution as the original incompressible formulation, provided the transients are slow and the flow Mach numbers are low. Although the new compressible formulation does not improve on the accuracy in the limit, it is certainly more accurate than the incompressible formulation for higher flow speeds and for faster transients. However, the biggest advantage of the new formulation is numerical robustness for fast transients where the original formulation simply fails due to numerical instability.